Mon. Not. R. Astron. Soc. **000**, 000–000 (0000) Printed 8 July 2011 (MN LATEX style file v2.2)

The Solar neighbourhood in angle coordinates: the Hyades moving group

Paul J. McMillan⋆
Rudolf Peierls Centre for Theoretical Physics, 1 Keble Road, Oxford, OX1 3NP, UK

arXiv:1107.1384v1 [astro-ph.GA] 7 Jul 2011

8 July 2011

ABSTRACT

I investigate the suggestion that the Hyades moving group in the Solar neighbourhood is the result of a recent inner Lindblad resonance. I use dynamical "torus" models of the Galaxy to understand the expected distribution of solar neighbourhood stars in angle coordinates for phase-mixed models and models which include a resonant component. I show that attempts to find the signatures of resonances in angle coordinates are strongly influenced by selection effects, including rather subtle effects associated with the relationship between action and angle for stars at a given point. These effects mean that one can not use simple tests to determine whether substructures seen in the Solar neighbourhood are associated with any given resonance.

Key words: solar neighbourhood – Galaxy: kinematics and dynamics – methods: data analysis

1 INTRODUCTION

Since Dehnen (1998) used proper motions and parallaxes obtained by the Hipparcos satellite (ESA 1997) to investigate the kinematics of the Solar neighbourhood, it has been clear that the local distribution function (DF) is far from smooth. In particular, the distribution of stars in the U, V plane[1] is dominated by a number of streams, all of which are thought to be dynamical in origin (e.g. Famaey et al. 2005).

Recently Sellwood (2010, henceforth S10) argued that part of this substructure could be explained by a recent inner Lindblad resonance (ILR), a conclusion he supported with reference to the distribution in angle coordinates of stars observed by the Geneva-Copenhagen survey (GCS: Holmberg, Nordström, & Andersen 2009). This conclusion was supported by Hahn, Sellwood, & Pryor (2011) who looked at stars in the Solar neighbourhood observed by the Radial Velocity Experiment (RAVE: Steinmetz et al. 2006) and the Sloan Digital Sky Survey (SDSS: Abazajian et al. 2009).

In this paper I reexamine S10's conclusion that the distribution of stars in the Solar neighbourhood show signs of an inner Lindblad resonance (ILR). I compare the GCS sample of stars in the Solar neighbourhood to a phase-mixed dynamical model. This allows me to separate selection effects from genuine substructure in the local DF, and to develop some understanding of the impact of selection effects on the observed properties of any substructure that is found in the local DF. I then explore the impact of selection effects on simple models of an ILR or an outer Lindblad resonance (OLR).

In Section 2 I discuss angle-action coordinates, how they might be used to determine the dynamical origin of observed kinematic substructure, and their relationship to kinematics in the Solar neighbourhood. In Section 3 I give numerical details of the assumptions made and the phase-mixed dynamical model considered. In Section 4 I explore the appearance in angle coordinates of the solar neighbourhood in a phase-mixed model, which I then use in Section 5 to interpret the distribution in angle coordinates of stars observed by the GCS. Section 6 discusses simple models which include a resonant component, and uses them to better understand the GCS data.

⋆ E-mail: p.mcmillan1@physics.ox.ac.uk

[1] Throughout this paper, in the Solar neighbourhood, velocities with respect to the Sun are described in terms of a component towards the Galactic Centre (U), a component in the direction of Galactic rotation (V), and a component perpendicular to the Galactic plane towards the north Galactic pole (W). Velocities with respect to the local standard of rest are described in terms of components in the same directions as U, V and W which are given the symbols v_x, v_y and v_z respectively

2 ANGLE-ACTION COORDINATES

Three actions J_i and three conjugate angle coordinates θ_i provide canonical coordinates for stars orbiting in the gravitational potential of the Galaxy. For a particle on any orbit the actions are conserved quantities and the angles increase linearly with time, $\theta_i(t) = \theta_i(0) + \Omega_i t$, where Ω_i is a frequency. This means that $\boldsymbol{J}$ can be thought of as labeling

an orbit, and $\boldsymbol{\theta}$ as describing a point on that orbit. The usual phase space coordinates $\boldsymbol{x}, \boldsymbol{v}$ are 2π-periodic in each angle coordinate θ_i. For a phase-mixed DF the distribution of stars is uniform in angle for any given range of actions, and therefore the DF $f = f(\boldsymbol{J})$.

The usage of angle-action coordinates has been somewhat limited by the fact that the relationship between $\boldsymbol{x}, \boldsymbol{v}$ and $\boldsymbol{\theta}, \boldsymbol{J}$ is only available analytically for a very limited set of gravitational potentials. I use the "torus-fitting" method (e.g. McMillan & Binney 2008) to find angle-action coordinates for stars with known velocities, and to construct a phase-mixed model. S10 found values for the angle-action coordinates in the plane using the approximation that the in-plane and vertical components of motion could be decoupled, and then integrating orbits in the plane. The torus method requires no such approximation, but since the stars being considered do not generally move far from the plane of the Galaxy, these approaches produce very similar results.

It was shown by S10 that stars trapped or scattered at a resonance with some perturbation in the potential will, at any given time, satisfy the relation

$$l\theta_r + m\theta_\phi \simeq const, \tag{1}$$

where the perturbation has m-fold rotational symmetry, and l is an integer or $l = \pm\frac{1}{2}$ for ultra-harmonic resonances. $l = -1$ corresponds to an ILR, $l = 1$ corresponds to an OLR, and $l = 0$ at corotation. The value of the constant in eq. 1 can take any value, and varies linearly with time. This condition is in addition to the usual condition for resonance

$$l\Omega_r + m\Omega_\phi = const = m\Omega_p, \tag{2}$$

where Ω_p is the pattern speed of the perturber, and l & m have the same meaning as before. This condition on frequency can also be thought of as being a condition on action, since $\boldsymbol{\Omega} = \boldsymbol{\Omega}(\boldsymbol{J})$

The zero-points for the angles can be defined arbitrarily (provide the same convention is applied for all orbits), and for clarity I follow the conventions used by S10. This means that each component of θ_i lies in the range $[-\pi, \pi]$. The Galactocentric coordinates are aligned such that the Sun is at a position in real space with Galactocentric coordinate $\phi = 0$. I take $\theta_r = 0$ at apocentre, and therefore $\theta_r = \pm\pi$ at pericentre. I define the zero point of θ_ϕ such that at apocentre $\theta_\phi = \phi$. Note that for small J_r, J_z, where it is appropriate to use the epicycle approximation, the value of θ_ϕ corresponds to the position (in ϕ) of the guiding centre.

Figure 1 is a schematic diagram illustrating the relationship between θ_r and θ_ϕ using the example of an orbit in the plane of the Galaxy with small eccentricity, where use of the epicycle approximation is appropriate. The star moves on an epicycle about the guiding centre, which is itself moving at a constant angular velocity. The radius of the orbit of the guiding centre about the galactic centre is determined by the angular momentum of the orbit. The size of the epicycle (i.e. a, the maximum radial excursion of the orbit away from the guiding centre and δ, the maximum value of $|\phi - \theta_\phi|$) can be found under the epicycle approximation

$$a \approx \sqrt{2J_r/\kappa} \tag{3}$$

and

$$\delta \approx \frac{2\Omega_c}{\kappa R_g} \times \sqrt{2J_r/\kappa}, \tag{4}$$

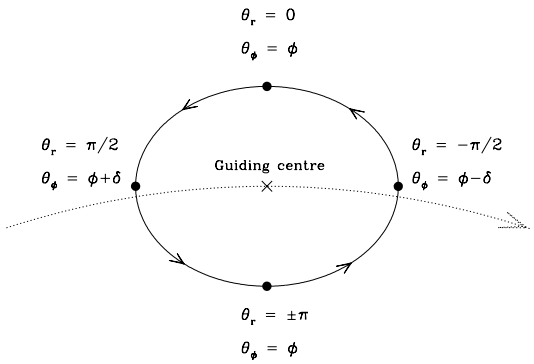

Figure 1. Schematic diagram illustrating the relationship between ϕ and θ_ϕ as a function of θ_r for low eccentricity orbits, for which the epicycle approximation applies. The *dotted* line and arrow shows the motion of the guiding centre (shown as a cross). The *solid* line and arrows show the motion of the star on an epicycle around the guiding centre. The maximum difference between ϕ and θ_ϕ is δ which can be found (under the epicycle approximation) using eq. 4. Note that the epicycle approximation is used purely for illustrative purposes in this paper, and is not used to find the relationship between $\boldsymbol{x}, \boldsymbol{v}$ and $\boldsymbol{\theta}, \boldsymbol{J}$.

where R_g is the radius of the guiding centre, $\Omega_c(J_\phi)$ is the circular frequency, and $\kappa(J_\phi)$ is the radial epicycle frequency (e.g. Binney & Tremaine 2008). For given value of $\boldsymbol{J}$ the value of θ_r sets the relationship between θ_ϕ and ϕ, and the orbit only goes through a given point (e.g. the Sun's position) at two values of $\boldsymbol{\theta}$ (related through $\theta_{r,1} = -\theta_{r,2}$, $\theta_{\phi,1} - \phi = \phi - \theta_{\phi,2}$).

In Figure 2 I show how values of J_r, J_ϕ, θ_r or θ_ϕ correspond to lines in the v_x, v_y-plane for stars that are exactly at the Sun's position, and for which we can ignore motion out of the plane (i.e. $J_z = 0$). As that plot shows, one can think of J_ϕ and θ_ϕ as providing near-Cartesian coordinate axes in the v_x, v_y-plane, and J_r and θ_r as providing near-polar coordinate axes in the v_x, v_y-plane. Indeed specifying any two values from the set $(J_r, J_\phi, \theta_r, \theta_\phi)$ defines a single position in the v_x, v_y-plane for a star at the Sun's position – except if the values are J_r and anything other than θ_r, in which case it can describe zero, one or two possible positions in the v_x, v_y-plane.

The stars considered in this paper are those found within 200 pc of the Sun, but none actually at the Sun's position, so the relationships between v_x, v_y and $\boldsymbol{J}, \boldsymbol{\theta}$ shown in Figure 2 are only approximate (even ignoring the motion out of the plane). A star being at Galactocentric $\phi = \phi_* \neq 0$ affects the value of θ_ϕ, shifting it by ϕ_* for a given v_x, v_y, with the greatest value of ϕ_* possible for this sample being ~ 0.02. A star being at $R \neq R_0$ affects the value of J_ϕ for a given v_x, v_y, but only by maximum of $\sim 0.02 J_{\phi,0}$ in this sample (with $J_{\phi,0}$ the angular momentum of a circular orbit at R_0). The values of J_r or θ_r for a given v_x, v_y are not significantly affected by the star's position within the solar neighbourhood, primarily because the circular velocity (and thus the velocity of a $J_r = 0$ orbit) barely changes across the volume considered for any reasonable Galactic potential.

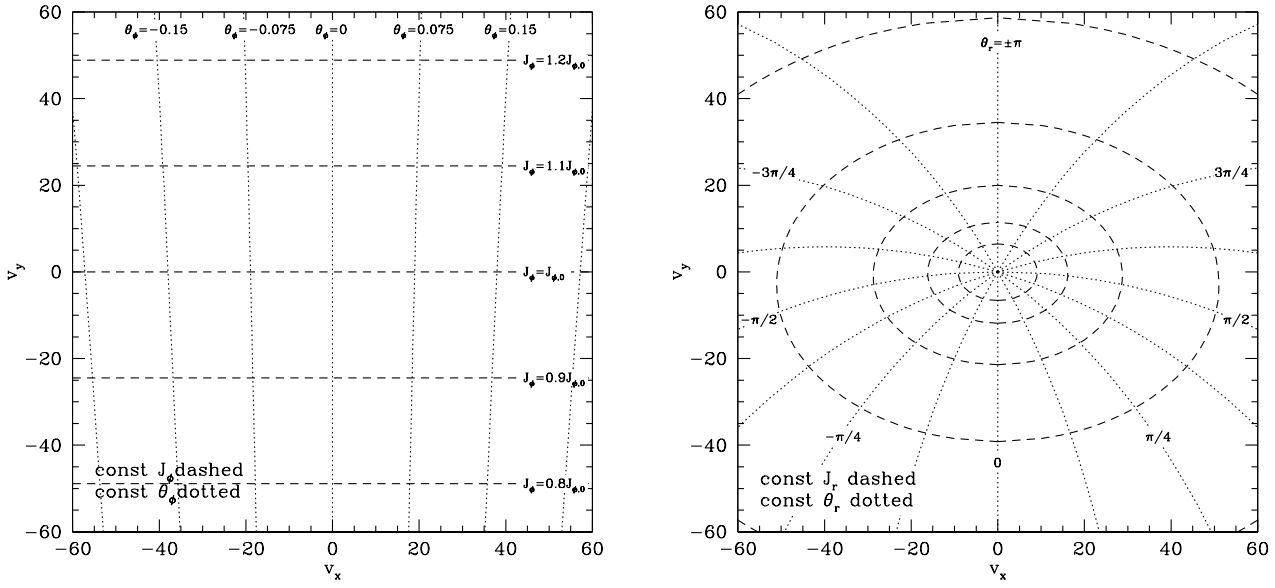

Figure 2. The v_x, v_y plane, with lines of constant θ_ϕ or J_ϕ (dotted and dashed respectively, left panel) or lines of constant θ_r or J_r (again dotted and dashed respectively, right panel) plotted, for a star at the Sun's position with $J_z = 0$. The lines of constant θ_ϕ and J_ϕ are linearly spaced in each case and labelled on the plot (where $J_{\phi,0} = 2080\,\mathrm{kpc\,km\,s^{-1}}$ is the angular momentum of a circular orbit at the Solar radius) – they form a nearly-Cartesian coordinate system for the v_x, v_y plane. The lines of constant θ_r are shown at intervals of $\pi/8$, with θ_r increasing as you move anti-clockwise on the plot. The lines of constant J_r are logarithmically spaced in J_r, with the innermost one at $1\,\mathrm{kpc\,km\,s^{-1}}$ and the value of J_r increasing by a factor of $\sqrt{10}$ at a time, with the outermost visible line corresponding to $J_r = 100\,\mathrm{kpc\,km\,s^{-1}}$. J_r and θ_r form a nearly-polar coordinate set in the v_x, v_y plane, with J_r as a "radius" and θ_r as a "polar angle".

The rest of this paper focuses on the distribution of stars in θ_r and θ_ϕ. I have examined the distribution of stars in θ_z and, apart from the expected tendency for stars to be at values of θ_z that place them near the Galactic plane (a selection effect), it shows no interesting features. This is entirely in keeping with the absence of kinematic substructure in v_z noted by Dehnen (1998), and S10's brief discussion of the J_z distribution.

3 NUMERICAL DETAILS

In all cases I use the "convenient" model Galactic potential given by McMillan (2011). This model consists of a bulge component, thin and thick exponential discs, and a Navarro, Frenk, & White (1996) halo. This sets the solar radius $R_0 = 8.5\,\mathrm{kpc}$ and the circular velocity at the Sun (the local standard of rest) $v_0 = 244.5\,\mathrm{km\,s^{-1}}$. I have explored the effect of using alternative Galactic potentials (including a logarithmic potential of the kind used by S10), and it does not significantly alter the main results.

I assume that the velocity of the Sun with respect to the local standard of rest is the best-fitting value found by Schönrich, Binney, & Dehnen (2010)

$$\boldsymbol{v}_\odot = (U_\odot, V_\odot, W_\odot) = (11.1, 12.24, 7.25)\,\mathrm{km\,s^{-1}}. \quad (5)$$

The phase-mixed model DF I compare to the real data is very similar to that described in Binney & McMillan (2011), but with altered disc scale-lengths (to reflect the scale-lengths of the discs that produce the potential). The thin and thick discs are modelled as having "quasi-isothermal" DFs, which is to say that they are of the form

$$f(J_r, J_\phi, J_z) = f_{\sigma_r}(J_r, J_\phi) \times \frac{\nu_z}{2\pi\sigma_z^2}\,\mathrm{e}^{-\nu_z J_z/\sigma_z^2}, \quad (6)$$

where

$$f_{\sigma_r}(J_r, J_\phi) \equiv \left.\frac{\Omega_\mathrm{c}\Sigma}{\pi\sigma_r^2\kappa}\right|_{R_\mathrm{c}} [1 + \tanh(J_\phi/L_0)]\mathrm{e}^{-\kappa J_r/\sigma_r^2}. \quad (7)$$

Here $\nu(J_\phi)$ is the vertical epicycle frequency and $\Sigma(J_\phi) = \Sigma_0 \mathrm{e}^{-(R_\mathrm{c}-R_0)/R_\mathrm{d}}$ is the (approximate) radial surface-density profile, where $R_\mathrm{c}(J_\phi)$ is the radius of the circular orbit with angular momentum J_ϕ. The factor $1+\tanh(J_\phi/L_0)$ in equation (7) is there to effectively eliminate stars on counter-rotating orbits and the value of L_0 is unimportant provided it is small compared to the angular momentum of the Sun. In equations (6) and (7) the functions $\sigma_z(J_\phi)$ and $\sigma_r(J_\phi)$ control the vertical and radial velocity dispersions, and I set

$$\begin{aligned}\sigma_r(J_\phi) &= \sigma_{r0}\,\mathrm{e}^{q(R_0-R_\mathrm{c})/R_\mathrm{d}}\\ \sigma_z(J_\phi) &= \sigma_{z0}\,\mathrm{e}^{q(R_0-R_\mathrm{c})/R_\mathrm{d}},\end{aligned} \quad (8)$$

where $q = 0.45$ and σ_{r0} and σ_{z0} are approximately equal to the radial and vertical velocity dispersions at the Sun. I take the DF of the entire disc to be the sum of a DF of the form (6) for the thin disc, and a similar DF for the thick disc, the normalisations being chosen so that at the Sun the surface density of thick-disc stars is 23 per cent of the total stellar surface density. Table 1 lists the parameters of each component of the DF.

The physical properties of the model are determined by both the DF and the Galactic potential and, as in Binney &

Table 1. Parameters of the DF.

Disc	R_d/kpc	$\sigma_{r0}/\mathrm{km\,s^{-1}}$	$\sigma_{z0}/\mathrm{km\,s^{-1}}$	$L_0/\mathrm{kpc\,km\,s^{-1}}$
Thin	3.0	27	20	10
Thick	3.5	48	44	10

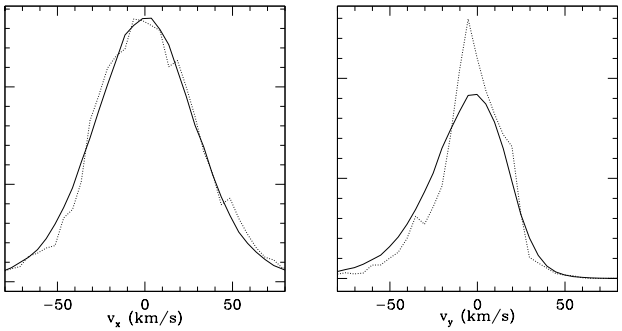

Figure 3. Distribution in v_x (*left*) and v_y (*right*) of stars observed by the GCS (assuming $\boldsymbol{v}_\odot$ is as given in eq. 5, *dotted* line) and taken from the solar neighbourhood in the phase-mixed model (*solid* line).

McMillan (2011), the DF does not self-consistently reproduce the potential. To produce a self-consistent dynamical model one has to specify a DF for the dark matter (which makes a substantial contribution to the potential), and distinguish carefully between the masses and luminosities of the stars. This lies well beyond the scope (or needs) of this study.

Samples of stars are produced by sampling the DF in $\boldsymbol{J}$, then sampling evenly in $\boldsymbol{\theta}$ in the range $[-\pi, \pi]$. This fully determines the position and velocity of the stars, and only those that lie within 200 pc of the Sun become part of the sample. This is the same procedure that was used in Binney & McMillan (2011) and, as in that paper, 200,000 values of $\boldsymbol{J}$ are sampled from the DF (all of which correspond to orbits that enter the solar neighbourhood) from which 1,000,000 stars in the solar neighbourhood are sampled.

In Figure 3 I plot the distribution of stars in v_x and in v_y from the GCS (assuming the value of $\boldsymbol{v}_\odot$ given in eq. 5) and from the phase-mixed DF. This simple DF does not entirely fit the observed data, in particular the GCS data has a much higher peak in its v_y distribution than the model data. However the v_x distributions are very similar and the model v_y-distribution is appropriately skew. Since this model is only being used as a guide, rather than as an attempt to reproduce the observed distributions, this is sufficient and I do not attempt to fit the observed distribution more precisely with DFs that are more complicated functions of the actions (e.g. Binney 2010).

4 APPEARANCE OF A PHASE-MIXED COMPONENT IN ANGLE COORDINATES

While, for a phase-mixed population, the distribution of stars in angle is uniform over any given range in action, it does not generally follow that the distribution is uniform over a given volume in real space. The distribution in angle of stars found within the Solar neighbourhood in a phase-mixed model is significantly non-uniform. In Figure 4 I show the distribution in θ_r and in θ_ϕ of stars in the solar neighbourhood, taken from the phase-mixed model.

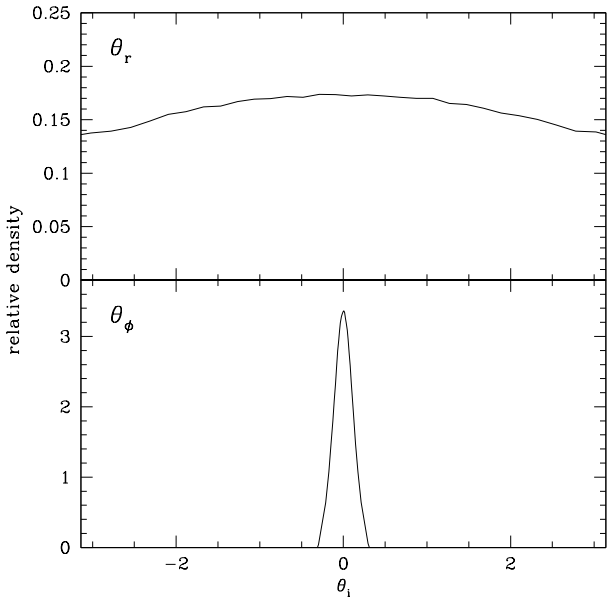

Figure 4. Distribution in θ_r (*upper*) and θ_ϕ (*lower*) of stars in the solar neighbourhood (radius of 200 pc) taken from the DF given in equation 6. These histograms, and all others in this paper showing the relative density of stars as a function of the angles, are normalised such that the total area under the histogram is unity, and are found by binning stars with bin width ~ 0.1 radians.

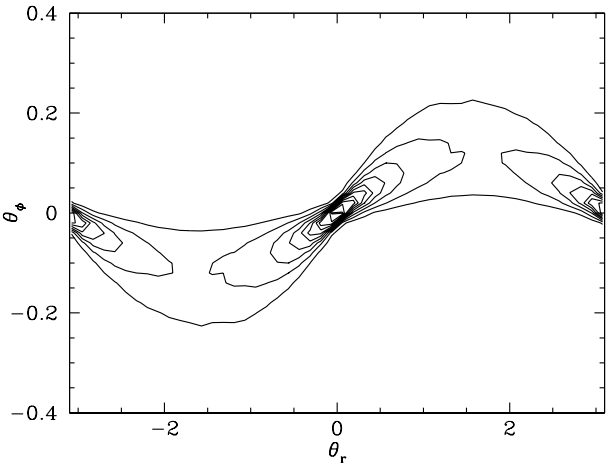

Figure 5. Contour plot showing the density in the θ_r, θ_ϕ plane of stars in the solar neighbourhood (radius of 200 pc) taken from the DF given in equation 6. Contours are spaced linearly in density. Note that the regions near $\theta_r = 0, \pm\pi$ have a high density because all stars near those points have $\phi \approx \theta_\phi$, and so stars in the solar neighbourhood have values of θ_ϕ that lie in a very small range (which does not vary with J_r).

The narrow distribution in θ_ϕ reflects the fact that the stars are taken from a very narrow range in ϕ, and that there is a close relationship between ϕ and θ_ϕ. The average

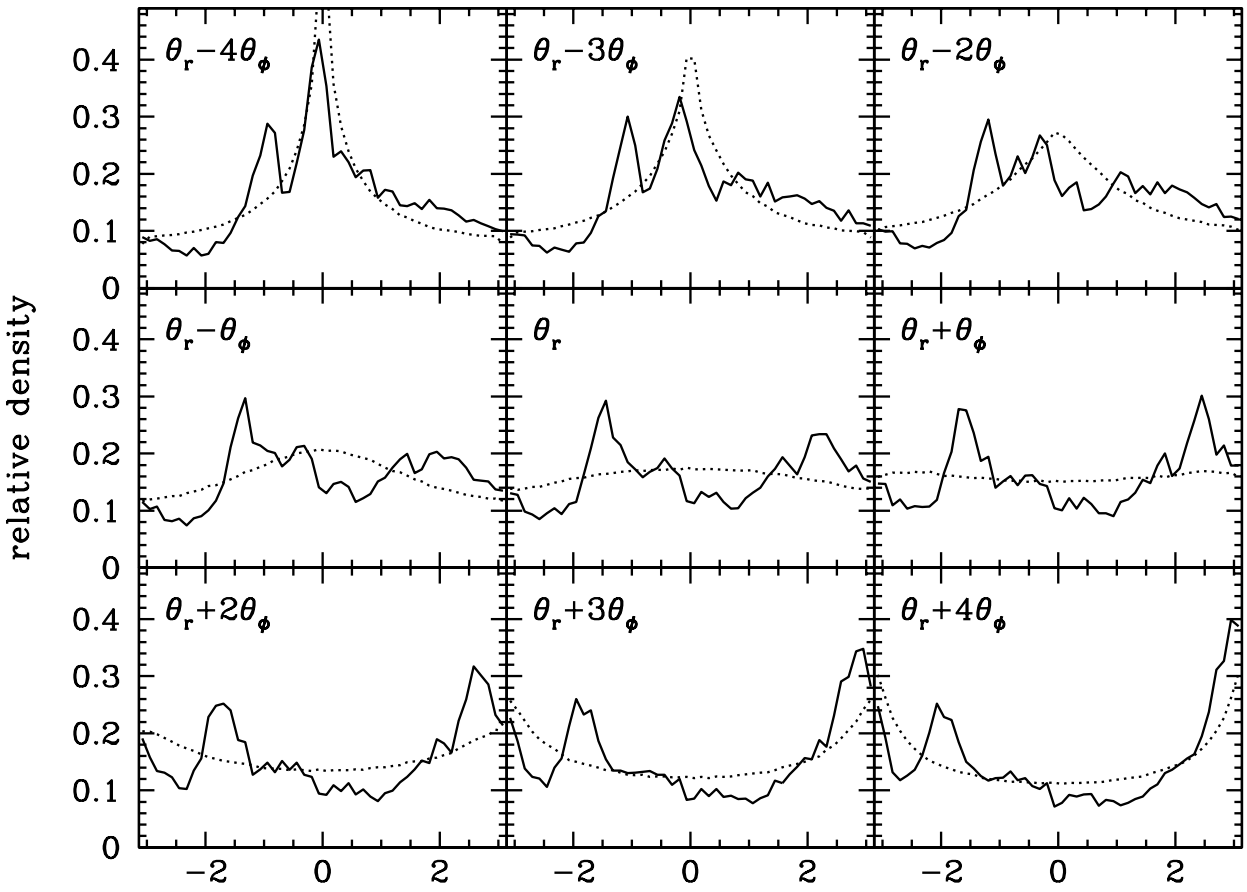

Figure 6. Plot showing the relative density of stars in the solar neighbourhood taken from my phase-mixed model (*dotted* line) and the GCS data (*solid* line) for the linear combinations of angles $\theta_r + n\theta_\phi$ for various values of n. The dotted line illustrates the effects of selection effects in each plot, so peaks in the solid line that are not seen in the dotted line are genuine substructure. ILRs are expected to produce peaks for $n < 0$ and OLRs to produce peaks for $n > 0$. The main features are (a) the peak visible in all plots that moves gradually with increasing n from $\theta_r - 4\theta_\phi \sim -1$ to $\theta_r + 4\theta_\phi \sim -2$; and (b) the peak that is only clearly visible for $n \geqslant 0$, moving with increasing n from $\theta_r \sim 2$ to $\theta_r + 4\theta_\phi \sim 3$. The movement and (to at least some extent) sharpening or broadening of the peaks is due to the selection effects seen in Figure 5.

value of δ (approximated using eq. 4) for stars in the survey volume is ~ 0.16.

The relative density of stars in θ_r is at a maximum around 0 (i.e. apocentre) and a minimum around $\pm\pi$ (pericentre). The stars at apocentre have guiding radii smaller than their current radius, and those at pericentre have guiding radii larger than their current radius. The excess of stars at apocentre is due to the fact that the density of stars, and their velocity dispersion, decreases with increasing radius, so more stars visit the Solar neighbourhood from guiding radii smaller than R_0 than from guiding radii larger than R_0. Since stars at apocentre are lagging circular rotation, while those at pericentre are leading it, this non-uniformity in the θ_r distribution is directly related to asymmetric drift, and the skew distribution in v_y seen in Figure 3 (e.g. Binney & Tremaine 2008). This behaviour is different from that suggested by S10 who incorrectly claimed that one should expect low relative density of stars around both $\theta_r = \pm\pi$ and $\theta_r = 0$.

In Figure 5 I show density contours for the values of θ_r and θ_ϕ taken from the phase-mixed model. There is a clear relationship between the two values, with $\theta_\phi \gtrsim 0$ for $\theta_r > 0$, and $\theta_\phi \lesssim 0$ for $\theta_r < 0$. There are extrema in θ_ϕ at $\theta_r = \pm\pi/2$, and $\theta_\phi \approx 0$ for $\theta_r = 0$ & $\pm\pi$. This is again due to the fact I am selecting stars from a very narrow range in ϕ, and because of the relationship between θ_r and θ_ϕ for a given orbit at a given point illustrated in Figures 1 and 2.

5 GENEVA COPENHAGEN SURVEY DATA

I now compare the phase-mixed model analysed in Section 4 to the stars in the Solar neighbourhood observed by the GCS. The GCS data are taken from the table produced by Holmberg et al. (2009), and I follow S10 in restricting the analysis to stars that have full 6D phase-space coordinates quoted, are at distances $\leqslant 200$ pc from the Sun, and are not directly associated with the Hyades cluster. The dis-

tributions in angle space that I find are very similar to those found by S10, and the small differences are due to the different choices of Galactic potential and the use of torus-fitting as opposed to integrating orbits in the plane.

In Figure 6 I plot the distributions in $\theta_r + n\theta_\phi$ of the GCS stars (solid line) and those taken from the phase-mixed model (dotted line) for a series of integers n. Naively one would simply expect an OLR to produce a peak for some value of $n > 0$, and an ILR to produce a peak for some value of $n < 0$ (with the perturber being $|n|$-fold symmetric). The relationship between θ_r and θ_ϕ due to selection effects produces a peak around 0 in plots with $n < 0$ and around $\pm\pi$ for $n > 0$. [2]

There are two main features in the angle distribution of the GCS data (besides those due to selection effects), one peak that lies at $\theta_r \sim -1.5$, and one that lies at $\theta_r \sim 2.2$. It is also noticeable that the peak at 0 which appears in the model data for $n < 0$ is offset to slightly lower values in the GCS data – this can be associated with the small peak in the θ_r distribution at $\theta_r \sim -0.4$.

Figure 7 shows the distribution of stars taken from the GCS data in the v_x, v_y-plane (assuming the Solar velocity relative to the local standard of rest given in eq. 5) overlaid on the lines of constant θ_r and of constant θ_ϕ (at the Sun's position) as shown in Figure 2. This makes it easy to see which of the familiar features in the v_x, v_y-plane correspond to which peaks in Figure 6. The peak at $\theta_r \sim -1.5$ is associated with the Hyades moving group, the peak at $\theta_r \sim 2.2$ is associated with the Sirius moving group and the peak at $\theta_r \sim -0.4$ is associated with the Pleiades moving group.

The peak at $\theta_r \sim -1.5$ clearly appears in all the plots shown in Figure 6, shifted to higher values for $n < 0$ and to lower values for $n > 0$. This peak is made up of almost the same set of stars in each plot. It is this feature that S10 identified as the signature of an ILR. It is clear from Figure 6 that these data are consistent with the stars that make up the peak at $\theta_r \sim -1.5$ being associated with any value of n between -4 and 4 (including non-integer values, and indeed for $|n| > 4$ though these are not shown as selection effects create ever greater distortions). While S10 shows plots that are almost identical to the centre and bottom-left panels of Figure 6 (his fig. 4 upper panel and fig. 7 top panel, respectively), the peaks in these plots are misidentified as being primarily due to selection effects that S10 incorrectly claimed should result in high relative densities around $\theta_r = \pm\pi/2$.

The peak at $\theta_r \sim 2.2$ becomes a more clearly defined (and higher) peak for $n > 0$ (shifted to higher values), and nearly disappears for $n < 0$. It is also noticeable that the feature around $\theta_r \sim -1.5$ becomes more sharply peaked for $n < 0$. This would seem to imply that the peak at $\theta_r \sim 2.2$ is associated with an OLR, and the peak at $\theta_r \sim -1.5$ is associated with an ILR, but this is not necessarily the case, both because of the selection effects discussed previously, and because of the other condition on resonant stars (eq. 2, see Section 6).

[2] The convention I use for these graphs means that for $n < 0$ they are mirror images of the comparable figures in S10. This choice is made so that the features in the various plots can easily be "followed" from one to another as n increases.

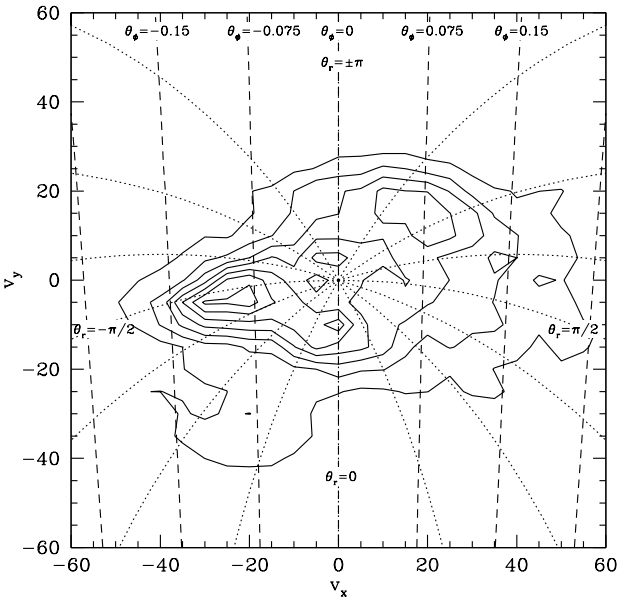

Figure 7. Distribution of GCS stars in the v_x, v_y-plane (*solid contours*), overlaid on lines of constant θ_r (*dotted*) and $theta_\phi$ (*dashed*) for stars at the Sun's position with $J_z = 0$, which are shown as a guide. This makes it easy to associate features seen in Figure 6 with the familiar Solar neighbourhood moving groups (e.g. Dehnen 1998). The Hyades moving group (around $v_x = -25\,\mathrm{km\,s^{-1}}$, $v_y = -5\,\mathrm{km\,s^{-1}}$) is clearly associated with the peak at $\theta_r \sim -1.5$. The Sirius moving group (around $v_x = 20\,\mathrm{km\,s^{-1}}$, $v_y = 15\,\mathrm{km\,s^{-1}}$) is associated with the peak at $\theta_r \sim 2.2$. The Pleiades moving group (around $v_x = -2\,\mathrm{km\,s^{-1}}$, $v_y = -10\,\mathrm{km\,s^{-1}}$ is associated with the peak near $\theta_r = -0.4$.

In Figure 8 I show a contour plot of the density in the θ_r, θ_ϕ plane of the selected stars from the GCS catalogue. The plots in Figure 6 are found from the distribution in angle space plotted in Figure 8 by marginalising it over straight lines, the gradient of which are determined by n. In Figure 8, lines corresponding to a few different values of n are plotted, centred on the main overdensities, to guide the eye.

The distribution in the θ_r, θ_ϕ plane seen in Figure 8 shows the same strong selection effects in $\boldsymbol{\theta}$ illustrated by the phase-mixed model. These selection effects have a very strong effect on the overdensities associated with the Pleiades and Sirius moving groups, which drives them towards the observed correlation between θ_r and θ_ϕ in the two different cases. The Hyades overdensity (around $\theta_r = -1.5$) is a less straightforward case. It is approximately triangular in the θ_r, θ_ϕ plane, and lies either side of the expected minimum in θ_ϕ at $\theta_r = -\pi/2$ (this minimum is seen in the phase-mixed model, Figure 5). The Hyades overdensity has increasing θ_ϕ with increasing θ_r for $\theta_r > -\pi/2$, and with decreasing θ_r for $\theta_r < -\pi/2$ (Figure 8), and these are the directions one would expect the selection effects that affected the phase-mixed model to drive the observations. This selection effect is important, but it is not clear that it is enough to explain the observed shape, and in Section 6 I explore the distribution in angle space of models with a resonant component.

Figure 9 shows a contour plot of the GCS data dis-

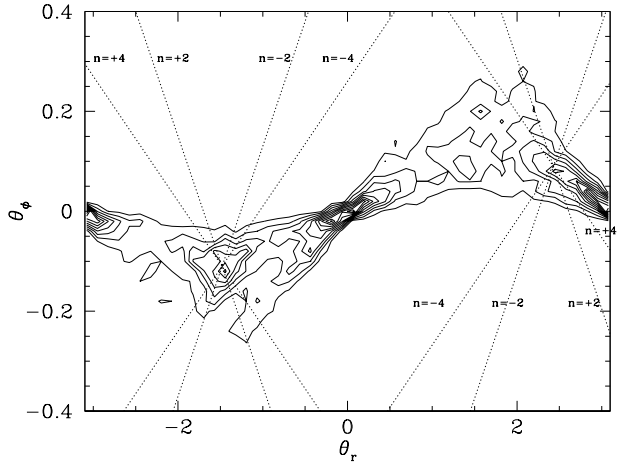

Figure 8. Contour plot of the density in the θ_r, θ_ϕ plane of stars taken from the GCS data (*solid* lines). Contours are spaced linearly in density, at the same densities as Figure 5 (relative to the total number of stars in each case). The various plots in Figure 6 can be thought of as being constructed from the density in this plane by marginalising over lines of constant $\theta_r + n\theta_\phi$. The *dotted* lines show these lines for $n = -4, -2, +2, +4$ passing through the main overdensities, to guide the eye.

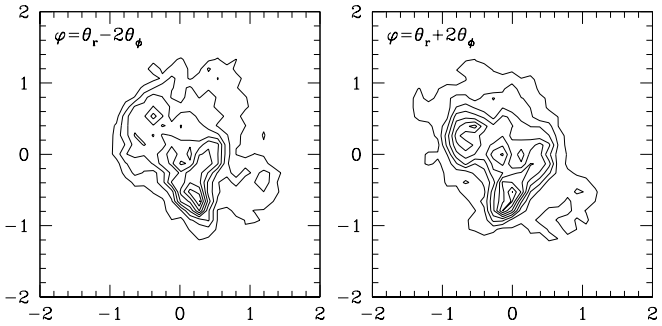

Figure 9. Contour plot showing the distribution of GCS stars in polar coordinates with radial coordinate a (eq. 3) the amplitude of radial motion under the epicycle approximation, and polar coordinate $\varphi = \theta_r + n\theta_\phi$ with $n = -2$ (*left*) or $n = 2$ (*right*). The overdensity corresponding to the Hyades is found around $(x, y) = (0.3, -0.6)$ in the $n = -2$ plot and around $(-0.05, -0.6)$ in the $n = 2$ plot. A plot very similar to the $n = -2$ one was shown by S10 as fig. 8.

tributed in polar coordinates with radial coordinate a (the amplitude of radial motion under the epicycle approximation, eq. 3) and polar coordinate $\varphi = \theta_r - 2\theta_\phi$ (left) or $\varphi = \theta_r + 2\theta_\phi$ (right). These are comparable to the upper panel of S10's fig. 8. In both cases one can see an overdensity at particular values of the polar coordinate, found (unsurprisingly) at the values of φ one would anticipate given Figure 6. S10 only showed a version of the plot with $\varphi = \theta_r - 2\theta_\phi$, finding that the plot for $\varphi = \theta_r + 2\theta_\phi$ (i.e. the plot that would suggest an OLR) argued against the suggestion that the Hyades corresponded to an OLR, primarily because the overdensity in the $\varphi = \theta_r - 2\theta_\phi$ plot appears to lie in a radial line out to larger a in the figure, whereas in the $\varphi = \theta_r + 2\theta_\phi$ plot it does not (Sellwood priv. comm.). This is not a particularly strong effect, but can be seen in

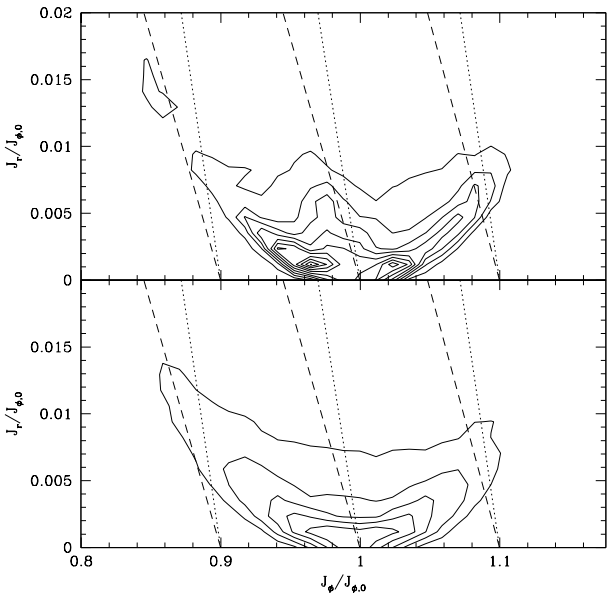

Figure 10. Contour plot of the density in the J_r, J_ϕ plane of stars taken from the GCS data (*solid* lines, *upper* plot), and of the phase-mixed model described in Section 3 (*solid* lines, *lower* plot). Contours are spaced linearly in density, at the same densities in each plot (relative to the total number of stars in each case). The Pleiades and Sirius moving groups produce small overdensities around $(J_r, J_\phi) = 0.96, 0.0015$ and $1.02, 0.0015$ respectively (in units where $J_{\phi,0} = 1$). The Hyades moving group produces a overdensity which is spread out in J_r at around $J_\phi = 0.97$, tending towards slightly lower J_ϕ with increasing J_r. Resonance lines for 2:1 OLRs (*dotted*) and ILRs (*dashed*) are plotted, where the value of Ω_p (eq. 2) is chosen in each case such that the lines reach $J_r = 0$ for $J_\phi = 0.9, 1$ and 1.1. A scatterplot of the distribution of the GCS stars in action was shown by S10 as fig. 3.

Figure 9, and understanding it requires moving beyond a phase-mixed model.

6 APPEARANCE OF AN OLR OR ILR IN ANGLE COORDINATES

Thus far in this study I have only considered two of the conditions on resonant stars – that they lie on or near lines of $l\theta_r + m\theta_\phi = const$ and that they must lie in the survey volume. To understand the expected distribution of resonant stars in a survey of the Solar neighbourhood, one must consider the combination of three different requirements on them:

- They must have angle coordinates near to a given resonance line in angle (eq. 1).
- They must have orbital frequencies (and thus actions) which place them near to a given resonance line in frequency (eq. 2).
- They must lie within the survey volume (e.g. within 200 pc of the Sun).

Note that over the Galaxy as a whole, the requirement on $\boldsymbol{\theta}$ only affects the distribution in $\boldsymbol{\theta}$ and the requirement on $\boldsymbol{J}$ only affects the distribution in $\boldsymbol{J}$ – the two distributions

can be thought of as independent[3]. It is only because of the finite survey volume, and therefore the finite range of $\boldsymbol{\theta}$ for which stars with for a given $\boldsymbol{J}$ will be observed, that the $\boldsymbol{J}$ condition significantly affects the observed $\boldsymbol{\theta}$ distribution (and vice versa).

In Figure 10 I plot the density of the GCS stars as a function of J_ϕ and J_r. The density of stars in my phase-mixed model is also plotted, for comparison. For a given J_ϕ there is a minimum $J_r = J_{r,min}$ for stars to reach the Solar neighbourhood, which can be thought of as a minimum epicyclic amplitude for a given guiding centre radius[4]. This is the cause of the near-parabolic lower boundary seen in Figure 10. The Pleiades and Sirius moving groups can be clearly seen as small overdensities in this plot. The Hyades moving group is seen as a rather more spread out overdensity at a range of J_r, around $J_\phi = 0.97 J_{\phi,0}$, tending towards slightly lower J_ϕ with increasing J_r.

The dotted and dashed lines in Figure 10 are 2:1 OLR and ILR lines respectively, these are lines along which $2\Omega_\phi(\boldsymbol{J}) + \Omega_r(\boldsymbol{J}) = 2\Omega_p$ and $2\Omega_\phi(\boldsymbol{J}) - \Omega_r(\boldsymbol{J}) = 2\Omega_p$ respectively, for different values of Ω_p, the perturber pattern speed, chosen such that the resonance lines reach $J_r = 0$ at $J_\phi = 0.9$, 1, or $1.1 J_{\phi,0}$. Changing the value of Ω_p moves the resonance lines in J_ϕ, but does not significantly alter their gradient in this range of $\boldsymbol{J}$. The Hyades overdensity seems to lie around a Lindblad resonance line, but this could be either an OLR or ILR line – it was this fact which lead S10 to claim this was an Lindblad resonance, but that one needed to investigate the distribution in angle to determine which one. Other resonances – the 3:1 or 4:1 OLR or ILR lines – would appear very similar on Figure 10, though the 2:1 ILR line is the furthest from the vertical. It is also worth noting that the slope of the various resonance lines is sensitive to the Galactic potential – in a logarithmic potential (of the kind used by S10), the gradients of the 2:1 OLR and ILR lines in this part of $\boldsymbol{J}$-space are nearly identical. It may be possible to use the slope of resonance lines in action space to provide information about the Galactic potential by comparing them to observed dynamical substructure, but that is beyond the scope of this study.

To explore the expected distribution of stars in the Solar neighbourhood associated with a resonance, I consider a DF related to the phase-mixed DF used previously, adjusted to include a resonant component:

$$f(\boldsymbol{J}, \boldsymbol{\theta}) \propto f_0(\boldsymbol{J}) \times (1 + C\, \eta_{res}(\boldsymbol{J}, \boldsymbol{\theta})) \quad (9)$$

where f_0 is the distribution function described in Section 3, C is a constant chosen such that the resonant component contributes 8 percent of the stars observed in the Solar neighbourhood, and

$$\eta_{res}(\boldsymbol{J}, \boldsymbol{\theta}) = \exp\left(-\frac{(J_\phi - J_{\phi,res})^2}{\Delta^2_{J,res}} - \frac{(\theta_r - \theta_{r,res})^2}{\Delta^2_{\theta,res}} \right). \quad (10)$$

$J_{\phi,res}$ is a function of J_r and is chosen such that $l\Omega_r(J_r, J_{\phi,res}) + m\Omega_\phi(J_r, J_{\phi,res}) = const$, for $J_z = 0$, and $\theta_{r,res}$ is a function of θ_ϕ and is chosen such that $l\theta_{r,res} + m\theta_\phi = const$. The values $\Delta_{J,res}$ and $\Delta_{\theta,res}$ give the width of the resonance peak around the exact resonance lines in J_ϕ and θ_r, respectively. One could, equally, describe the width in action or angle in terms of a spread in J_r or θ_ϕ respectively, but for convenience I have chosen to describe it in terms of the coordinates with the greater ranges of values in these data. The width $\Delta_{J,res}$ is effectively a width in frequency about the pattern speed of the perturber. In the toy models I show here I take $\Delta_{J,res} = 0.01 J_{\phi,0}$, $\Delta_{\theta,res} = 0.3$.

I consider two toy models, each designed to produce models with an overdensity in phase-space in a similar volume to that where the Hyades moving group is found (but not tuned to produce a best fit), one corresponding to an OLR ($l = 1$, $m = 2$) and one corresponding to an ILR ($l = -1$, $m = 2$). For the OLR model, I take $\theta_{r,res} + 2\theta_\phi = -1.9$, and for the ILR model $-\theta_{r,res} + 2\theta_\phi = 1.3$. In the OLR case I take $J_{\phi,res}(J_r = 0) = 0.975 J_{\phi,0}$, and in the ILR case $J_{\phi,res}(J_r = 0) = 0.985 J_{\phi,0}$.

Figure 11 shows contour plots of the density in the θ_r, θ_ϕ plane of the OLR and ILR models, and plots of $\theta_r + n\theta_\phi$ (as in Figure 6) restricted to $n = \pm 2$ in the interests of brevity. Both the ILR and OLR models reproduce some of the features of the Hyades overdensity. In both cases the overdensity in angle space is somewhat triangular in shape, like the Hyades overdensity, rather than following a single line as one would expect if only the condition on angle (eq. 1) was relevant. In both cases the overdensity in angle is strong for the two cases $n = \pm 2$, as well for other values of n (not shown).

In an effort to explain the structure of the overdensity in the θ_r, θ_ϕ plane, the upper panels of Figure 11 also show the lines $\theta_r = \theta_{r,res}$ for the two models, and lines corresponding to the condition on $\boldsymbol{J}$. The latter are found by taking the condition that $J_\phi = J_{\phi,res}(J_r)$ (or $J_\phi = J_{\phi,res} \pm \Delta_{J,res}$ or $J_\phi = J_{\phi,res} \pm 2\Delta_{J,res}$) and determining the two possible values of $\boldsymbol{\theta}$ that a star with these actions would have at the Sun's position – in the relevant part of phase space, lower values of J_r correspond to smaller (i.e. closer to zero) values of θ_ϕ. This gives a sense of the two competing effects which (in addition to the general selection effects illustrated in Figure 5) determine the shape of the overdensity in angle space, but it is important to also consider the effect of the finite volume surveyed on the constraint applied by the condition on $\boldsymbol{J}$, i.e. how close to the dotted lines in Figure 11 stars must actually lie.

A star with a given value of $\boldsymbol{J}$ which lies within 200 pc of the Sun will have a value θ_ϕ which lies within ~ 0.02 of the value for a star *at* the Sun, while the range of possible values of θ_r is typically larger, and increases with decreasing J_r (and thus, in the overdensity considered, with decreasing θ_ϕ). This latter point can be understood by considering a star in the epicycle approximation. As $J_r \to 0$ the epicycle shrinks to negligible size, so the star can be at any point on

[3] In practice they are not entirely independent – the resonant stars at the (say) higher values of $l\theta_r + m\theta_\phi$ about the resonance are probably there *because* they have the higher values of $l\Omega_r(\boldsymbol{J}) + m\Omega_\phi(\boldsymbol{J})$. This effect is likely to have some impact, but is beyond the scope of this study

[4] For a given J_ϕ, the value of $J_{r,min}$ is in fact dependent on J_z, with increasing J_z generally causing a decrease in $J_{r,min}$ if $J_\phi < J_{\phi,SN}$, and an increase in $J_{r,min}$ if $J_\phi > J_{\phi,SN}$, where $J_{\phi,SN}$ is the angular momentum of a circular orbit that passes through the Solar neighbourhood. This effect is small for the stars considered here as they have $J_z \ll J_\phi$.

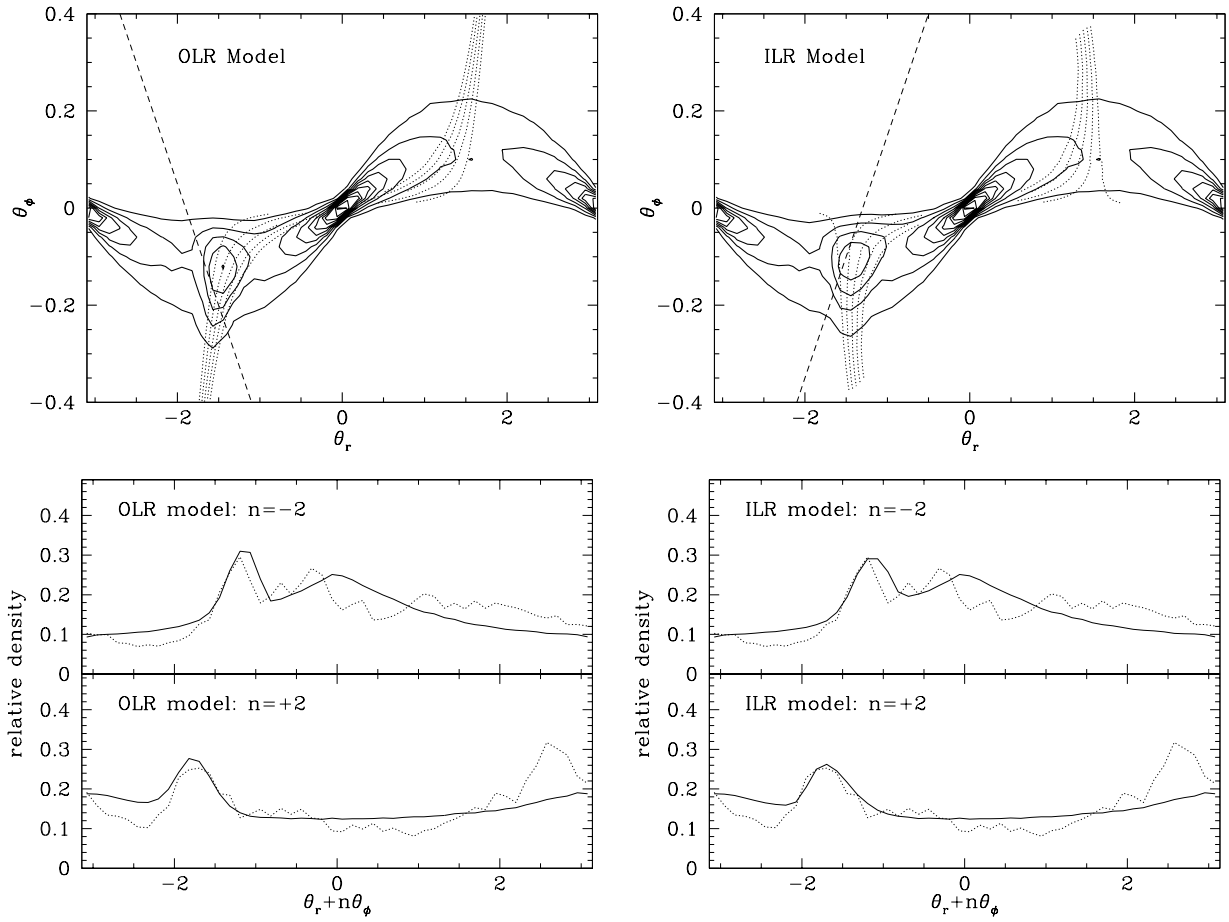

Figure 11. Plots showing the distribution of stars in $\boldsymbol{\theta}$ of stars taken from the OLR (*left*) and ILR (*right*) models. The upper panels show a contour plot of the density in the θ_r, θ_ϕ plane (*solid* line). The *dashed* line in those figures is the line $\theta_r = \theta_{r,res}(\theta_\phi)$ (eq. 10), and the *dotted* lines are the angle coordinates corresponding to the resonance lines in action at the Sun's position – as discussed in Section 2 a position and value of $\boldsymbol{J}$ defines two possible values of $\boldsymbol{\theta}$. In either set of five dotted lines, the central one corresponds to $J_\phi = J_{\phi,res}(J_r)$, and those either side correspond to $\pm\Delta_{J,res}$ and $\pm 2\Delta_{J,res}$. The lower panels show the distribution of stars in $\theta_r + n\theta_\phi$, as in Figure 6 except restricted to only $n = -2$ or 2. In this case the *solid* line shows the distribution for the model, and the *dotted* line shows the distribution for the GCS stars (for comparison).

the epicycle (therefore any θ_r) and still be within the survey volume if the value of θ_ϕ is one that places it there. As J_r increases, and the epicycle increases in size, the fraction of the epicycle (i.e. the range in θ_r) that corresponds to stars that enter the survey volume decreases.

Figure 12 shows polar plots, analogous to those in Figure 9, each labeled with which model they represent and what was used as the polar angle φ (the radial coordinate, as before, is always radial epicycle amplitude a). In each case I again plot the lines corresponding to $\theta_r = \theta_{r,res}(\theta_\phi)$ and $J_\phi = J_{\phi,res}(J_r)$, evaluated at the Sun's position. Once again, it is clear that both resonant conditions are important on the distribution in these plots, so the overdensity seen will be distorted away from $\theta_r + n\theta_\phi = const$ even if the model has $\theta_{r,res} + n\theta_\phi = const$ as a constraint, providing there is a non-negligible width around the resonance in $\boldsymbol{\theta}$.

Note that as J_r increases (and the size of the epicycle increases), the condition on $\boldsymbol{J}$ becomes more restrictive in $\boldsymbol{\theta}$ for the reason discussed above. Therefore this condition becomes increasingly dominant on the observed overdensity. This can be seen in Figure 12 as the outer contours show that the overdensity appears to follow the dotted line corresponding to $J_\phi = J_{\phi,res}(J_r)$ at large J_r. For *both* of the models this means that the contours seem to show an overdensity that lies around a value of $\theta_r - 2\theta_\phi$ that is approximately constant with increasing J_r, while lying around a value of $\theta_r + 2\theta_\phi$ that varies with increasing J_r. This provides a natural explanation for the slight curvature as J_r increases of the overdensity associated with the Hyades moving group in the equivalent plot for the GCS stars (Figure 9) – for overdensities produced by either an OLR or ILR, this curvature is seen as a result of the selection effects and the constraint in $\boldsymbol{J}$.

I have explored models with resonances at other frequency ratios (and thus with different relationships between θ_r and θ_ϕ), and found that it is possible to produce overdensities in $\boldsymbol{\theta}$ that are qualitatively very similar to those shown here. While it may be possible to tell one from another for given observations (such as those of the Hyades) it is certainly a very complicated task, and one that will require careful modelling and analysis.

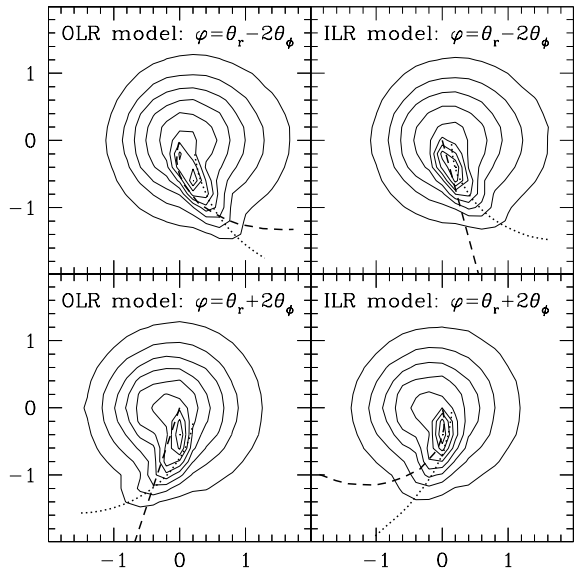

Figure 12. Contour plot showing the distribution of stars from the OLR (*left*) and ILR (*right*) models in polar coordinates with radial coordinate a, the amplitude of radial motion in the epicycle approximation, and polar coordinate $\varphi = \theta_r + n\theta_\phi$ with $n = -2$ (*upper*) or $n = 2$ (*lower*). The *dashed* lines are given by $\theta_r = \theta_{r,res}(\theta_\phi)$ (eq. 10) for the given model, evaluated at the Sun's position (so that the value of $\boldsymbol{\theta}$ determines a value of $\boldsymbol{J}$). The *dotted* lines are given by $J_\phi = J_\phi(J_{r,res})$ for the given model, again evaluated at the Sun's position.

7 DISCUSSION AND CONCLUSIONS

In this paper I have re-examined the distribution of stars in the Solar neighbourhood in angle coordinates following the claim by S10 that the Hyades moving group is related to an ILR. Using a dynamical "torus" model I showed the significant impact of selection effects associated with surveying a finite (small) volume upon the distribution of stars in angle coordinates taken from a phase-mixed model. Using models which contain resonant components in addition to a phase-mixed background I have demonstrated the important effects that the distribution of resonant stars in action have on the observed distribution in angle (again because of selection effects).

The distribution of the stars associated with the Hyades moving group in action (Figure 10) indicates that it is associated with some resonance between the radial oscillations and the azimuthal motion (i.e. follows a relation of the form of $l\Omega_r + m\Omega_\phi$). It is also clear that the stars which make up the resonant component are constrained in $\boldsymbol{\theta}$ in some way, otherwise there would be an overdensity at $\theta_r \sim 1.5$ as well as $\theta_r \sim -1.5$. However, it is very difficult to determine what the values of l and m are, and thus which resonance is responsible. In action space the lines $l\Omega_r(\boldsymbol{J}) + m\Omega_\phi(\boldsymbol{J}) = const$ are very similar, in the relevant range of $\boldsymbol{J}$, for different values of l and m, and are sensitive to choice of the Galactic potential. The approach taken by S10, of looking for overdensities in the statistic $l\theta_r + m\theta_\phi$, is also flawed because of the selection effects that have important influences on the distribution in $\boldsymbol{\theta}$. I find that, contrary to the conclusions of S10, it not clear that the Hyades moving group is the result of an inner Lindblad resonance.

It may be possible to use careful modeling and analysis, which takes into account selection effects and the distributions in $\boldsymbol{\theta}$ and $\boldsymbol{J}$ simultaneously, to determine what type of resonance is responsible for the Hyades moving group from these data. However this task is made even more difficult by uncertainty about the Galactic potential which significantly affects the gradient of resonance lines in action space.

It seems likely the problems of selection effects in studies of this kind will prove extremely challenging, if not intractable, while we are dealing with survey volumes corresponding to the relatively small radii ($\sim 200\,\mathrm{pc}$) associated with the GCS. To go beyond this with similar accuracy (i.e. $\sim 1\,\mathrm{km\,s^{-1}}$ velocity uncertainty) requires distance and proper measurements more accurate than those currently available – the RAVE and SDSS data used by Hahn et al. (2011) has significantly larger uncertainties even though they select stars which lie in the same volume as the GCS stars. Gaia (Perryman et al. 2001) is expected to produce 3-dimensional velocity measurements accurate to $\sim 1\,\mathrm{km\,s^{-1}}$ for some stars up to $\sim 3\,\mathrm{kpc}$ from the Sun, corresponding to a range in Galactocentric ϕ of order 0.7 radians. This will dramatically reduce the impact of selection effects on the observed distributions in angle-action coordinates, and should make it relatively straightforward to pick out structures in angle space that are unambiguously of the kind predicted by S10. This process is likely to both be guided by and affect the determination of the gravitational potential of the Galaxy (an essential product of the Gaia mission).

Throughout this study I have assumed that the uncertainties on the positions and velocities of the stars observed by the GCS can be ignored, because they are too small to have any significant effect. It is worth noting that the relationship between the uncertainty in $\boldsymbol{x}, \boldsymbol{v}$ and that in $\boldsymbol{\theta}, \boldsymbol{J}$ is not entirely straightforward, and that a small uncertainty in velocity does not necessarily correspond to a small uncertainty in $\boldsymbol{\theta}$. As inspection of Figure 2 suggests, the relationship between an uncertainty in velocity and that in θ_r is heavily dependent on J_r, with smaller J_r corresponding to a greater uncertainty in θ_r for given uncertainty in $\boldsymbol{v}$. Indeed as $J_r \to 0$ a negligible uncertainty in $\boldsymbol{v}$ corresponds to an uncertainty of 2π in θ_r. The Hyades overdensity does not extend to $J_r = 0$ (as can be seen in Figure 7), so the assumption that the uncertainty in θ_r can be ignored is reasonable for this study. However, future efforts to understand resonances of this type is likely to require appropriate treatment of these uncertainties.

ACKNOWLEDGMENTS

I thank members of the Oxford dynamics group for helpful input, especially James Binney for careful reading of an early draft of this paper. I am also grateful to Jerry Sellwood for a very helpful discussion which provoked the work described in Section 6. This work is supported by a grant from the Science and Technology Facilities Council.

REFERENCES

Abazajian K. N., Adelman-McCarthy J. K., Agüeros M. A., et al., 2009, ApJS, 182, 543
Binney J., 2010, MNRAS, 401, 2318
Binney J., McMillan P., 2011, MNRAS, 413, 1889
Binney J., Tremaine S., 2008, Galactic Dynamics: Second Edition. Princeton University Press
Dehnen W., 1998, AJ, 115, 2384
ESA, 1997, VizieR Online Data Catalog, 1239, 0
Famaey B., Jorissen A., Luri X., Mayor M., Udry S., Dejonghe H., Turon C., 2005, A&A, 430, 165
Hahn C. H., Sellwood J. A., Pryor C., 2011, arXiv:1102.4626
Holmberg J., Nordström B., Andersen J., 2009, A&A, 501, 941
McMillan P. J., 2011, MNRAS, 414, 2446
McMillan P. J., Binney J. J., 2008, MNRAS, 390, 429
Navarro J. F., Frenk C. S., White S. D. M., 1996, ApJ, 462, 563
Perryman M. A. C., de Boer K. S., Gilmore G., Høg E., Lattanzi M. G., Lindegren L., Luri X., Mignard F., Pace O., de Zeeuw P. T., 2001, A&A, 369, 339
Schönrich R., Binney J., Dehnen W., 2010, MNRAS, 403, 1829
Sellwood J. A., 2010, MNRAS, 409, 145
Steinmetz M., Zwitter T., Siebert A., et al., 2006, AJ, 132, 1645